MULTIPACTOR BREAKDOWN IN OPEN TWO-WIRE TRANSMISSION LINES

Joel Rasch [(1)], Dan Anderson [(2)] , Joakim Johansson [(3)], Mietek Lisak [(4)], Jerome Puech [(5)], Elena Rakova [(6)], Vladimir E. Semenov [(7)]

[(1)] Chalmers University of Technology, SE-412 96 Gothenburg, Sweden, Email: joel.rasch@chalmers.se
[(2)] Chalmers University of Technology, SE-412 96 Gothenburg, Sweden, Email: elfda@chalmers.se
[(3)] RUAG Space AB, SE-415 05 Gothenburg, Sweden, Email: joakim.johansson@ruag.com
[(4)] Chalmers University of Technology, SE-412 96 Gothenburg, Sweden, Email: elfml@chalmers.se
[(5)] Centre National d'Études Spatiales, 31401 Toulouse CEDEX 9, France, Email: jerome.puech@cnes.fr
[(6)] Institute of Applied Physics, R.A.S., 603600 Nizhny Novgorod, Russia, Email: eir@appl.sci-nnov.ru
[(7)] Institute of Applied Physics, R.A.S., 603600 Nizhny Novgorod, Russia, Email: sss@appl.sci-nnov.ru

ABSTRACT

Present guidelines for multipactor susceptibility assessment (*e.g.* ECSS) are based on a simplified representation of the actual device design in terms of a parallel plate geometry. When applied to open structures, *e.g.* balanced transmission lines and quadrifilar helix antennas, this produces overly conservative estimates of the multipactor susceptibility.

A simplified TEM transmission line geometry consisting of two cylindrical conductors has been studied. The convex conductor shape is shown to lead to a geometrically induced dilution of the electron density during successive passages between the conductors. This effect is equivalent to a loss of electrons and significantly reduces the probability of multipactor.

A simple susceptibility chart has been constructed that shows the parameter combinations for which multipactor cannot occur and gives an estimate of the susceptibility as compared to the simplified parallel plate case approximation.

1. INTRODUCTION

The present trend towards higher data rates in all kinds of space communication applications necessitates higher RF power levels to maintain a sufficient carrier-to-noise ratio. The increase of carrier power combined with the demanding space environment results in serious power handling issues in antennas, transmission lines, and related components.

Microwave breakdown due to multipactor and corona has long been recognized as a potential problem in RF space applications. Breakdown can occur during ambient pressure ground testing, during the launch ascent phase, or in the high vacuum environment in orbit. Multipactor in high vacuum will typically be dimensioning for the design, except for the case when the transmitter is switched on during ascent and thus intermediate pressure corona can occur.

A considerable amount of research and development has been put into analyzing and mitigating multipactor. Much of the effort has been directed to model the surface physics of the materials involved, especially the secondary emission yield (SEY). In order to maintain as few parameters as possible in the analysis, the canonical case of a parallel plate structure is typically considered.

A few transmission line and filter component structures, such as coaxial lines [1, 2], rectangular [3, 4] and circular waveguides [5], and irises [6], have been studied in detail. For more complicated structures, *ad hoc* numerical models are needed to investigate the specific problem.

Guidelines, such as the ECSS standard [7], exist for the analysis and testing of multipactor. The guidelines are heavily dependent on the parallel plate assumption, and would typically lead to overly conservative estimates regarding the breakdown susceptibility. Not having reliable prediction tools could lead to non-optimal trade-offs during the engineering design phase, and could lead to unnecessary testing with consequences to project schedule and budget.

Hitherto, little has been published on multipactor in open structures, such as the balanced two-wire TEM transmission line and the helix antenna shown in Fig. 1.

There are some important factors that distinguish this type of geometry from the canonical parallel-plate one:

- The structure is open, and there is a high probability for electrons being ejected and not impacting on the structure again.
- The field strength is inhomogeneous in the direction of the line between the conductor centers.
- The field strength is inhomogeneous in the direction perpendicular to the line between the conductor centers.

All these factors will contribute to a significant increase in the multipactor breakdown threshold voltage, which will be established in the following sections.

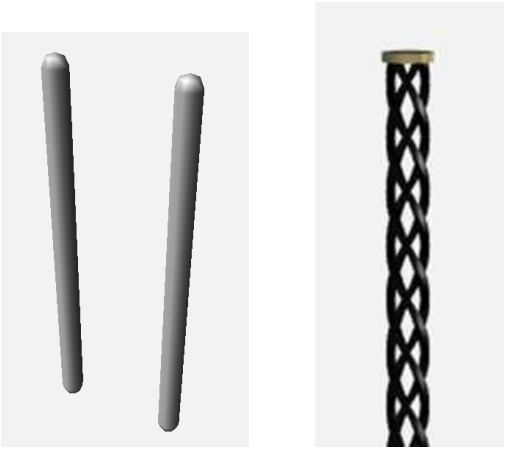

Figure 1. Examples of open structures: Two wire transmission line (left) and quadrifilar helix antenna (right).

2. THE TWO-WIRE TEM LINE

The circular cross-section two-wire TEM transmission line is a very convenient choice for a canonical structure. The field is known in closed form from logarithmic potential theory (see *e.g.* [8]). In Fig. 2, the equipotential curves for two parallel filamentary sources are shown. The equipotential curves and field lines are circles (or straight lines in some limit cases).

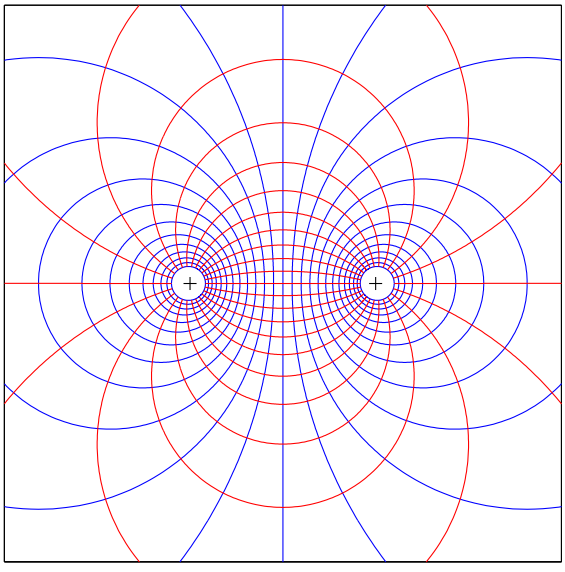

Figure 2. The equipotential curves (blue) and field lines (red) for a pair of filamentary line sources.

By a judicious choice of the circles it is seen that the dual filament case can be used to model *all* circular cross-section two-wire and coaxial lines, including various combinations of eccentricity and asymmetry (see Fig. 3). The parallel plate case can also be included as a limiting case.

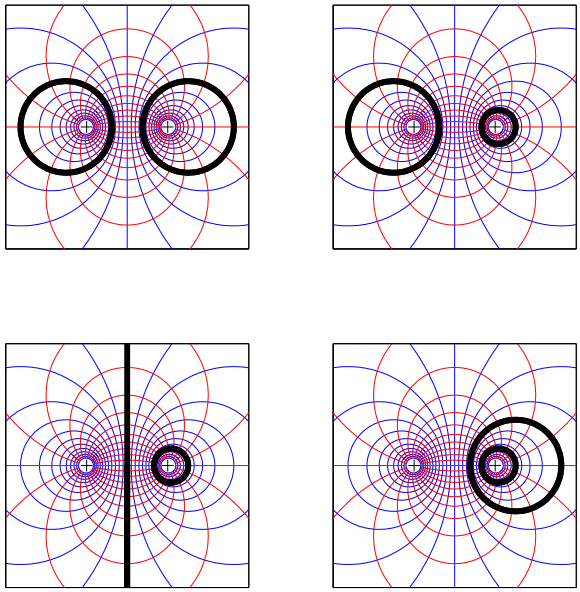

Figure 3. A judicious choice of equipotential curves can model symmetric (top left) and asymmetric two-wire lines (top right), line over ground-plane (bottom left), and eccentric coaxial lines (bottom right).

One advantage with using the TEM line approach is to separate the problem into a wave solution in the direction of the line, and thus just having a two-dimensional problem in the transversal direction, *viz.*

$$\boldsymbol{\mathcal{E}}(\mathbf{r},t) = \mathrm{Re}\left\{\mathbf{E}(x,y)\,e^{j[\omega t+\varphi_o \mp kz]}\right\} \tag{1}$$

$$\boldsymbol{\mathcal{H}}(\mathbf{r},t) = \pm\hat{z}\times\mathrm{Re}\left\{\frac{\mathbf{E}(x,y)}{\eta_o}\,e^{j[\omega t+\varphi_o \mp kz]}\right\} \tag{2}$$

Using the notation in Fig. 4, one can show that

$$\Delta = \frac{1}{D}\sqrt{\left(D^2 - R_1^2 - R_2^2\right)^2 - \left(2R_1R_2\right)^2} \tag{3a}$$

$$\delta_1 = \frac{1}{2D}\left(D^2 + R_1^2 - R_2^2\right) - \frac{\Delta}{2} \tag{3b}$$

$$\delta_2 = \frac{1}{2D}\left(D^2 - R_1^2 + R_2^2\right) - \frac{\Delta}{2} \tag{3c}$$

and the electrical field is given by

$$\mathbf{E} = \frac{E_o}{4} \frac{\left(\eta^2 - \xi^2 + 1/4\right)\hat{x} - 2\xi\eta\,\hat{y}}{\left(\eta^2 + \xi^2 - 1/4\right)^2 + \eta^2} \qquad (4a)$$

$$\xi = \frac{x}{\Delta} \quad \eta = \frac{y}{\Delta} \qquad (4b)$$

$$E_o = \frac{4V}{\Delta} \Big/ \operatorname{arccosh} \frac{D^2 - R_1^2 - R_2^2}{2R_1R_2} \qquad (4c)$$

V is here denoting the voltage between the conductors, and ρ_l is the filamentary linear charge density.

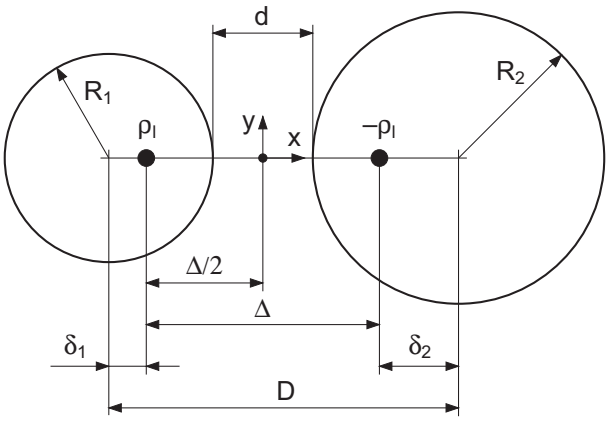

Figure 4. The two-wire TEM line geometry definition.

The circular cross-section two-wire geometries can be presented in a parameter plane, representing the conductor radii in terms of the conductor distance, see Fig. 5. By allowing the radii R_1 and R_2 in Eqs. 3-4 to assume negative and/or infinite values, it is also possible to include symmetric and eccentric coaxial lines, line over ground-plane, as well the parallel plate case.

The parametric contour for the symmetric coaxial line case is given by

$$\left(1 + d/R_1\right)\left(1 + d/R_2\right) = 1 \qquad (5)$$

and the parallel plate case by

$$d/R_1 = d/R_2 \equiv 0 \qquad (6)$$

The area below the coaxial line contour in Fig. 5 is a "forbidden" region, since the conductors would intersect for those parameter combinations.

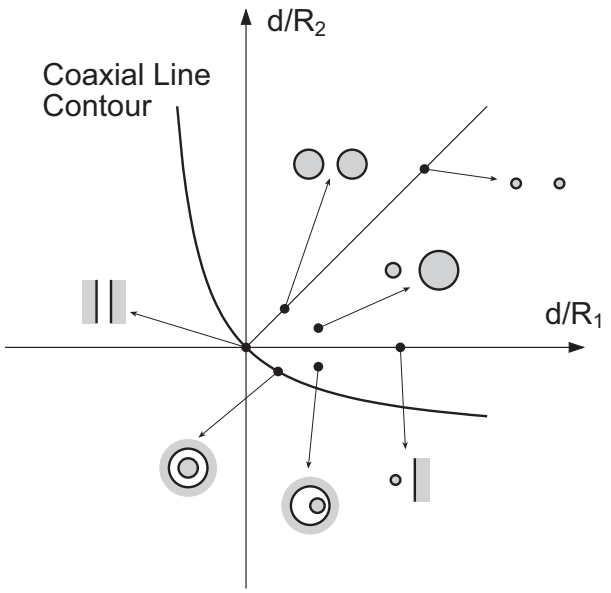

Figure 5. The parameter plane for various two-wire geometries.

3. ANALYSIS

3.1. A Ponderomotive Model

When analyzing the motion of the electrons, the complete approach would be to use Newton's law of motion together with the Lorentz force created by the electric and magnetic fields, *viz.*

$$m\,\ddot{\mathbf{r}} = -e\left(\boldsymbol{\mathcal{E}}(\mathbf{r},t) + \dot{\mathbf{r}} \times \boldsymbol{\mathcal{B}}(\mathbf{r},t)\right) \qquad (7)$$

Typically one can neglect relativistic effects and the magnetic field component, since multipactor would occur for much lower velocities. However, a fully numerical approach gives little insight into the multipactor physics, and a semi-analytical approach is conveniently used. In this approach, the motion of the electron is separated into an oscillatory part, the amplitude of which will be dependent on the spatially averaged field strength, and a slow drift velocity part, *viz.*

$$\mathbf{r}(t) = \tilde{\mathbf{r}}(t) + \mathbf{R}(t) \qquad (8a)$$

$$\tilde{\mathbf{r}} = \frac{e}{m\omega^2}\mathbf{E}(\mathbf{R})\cos\left(\omega t + \varphi_o\right) \qquad (8b)$$

It is convenient to introduce an oscillation peak velocity $\mathbf{v}_\omega$:

$$\dot{\tilde{\mathbf{r}}} = -\,\mathbf{v}_\omega \sin\left(\omega t + \varphi_o\right) \quad \mathbf{v}_\omega = \frac{e\,\mathbf{E}(\mathbf{R})}{m\omega} \qquad (9)$$

In the parallel-plate case the drift velocity is constant, but in the general case the field inhomogeneities create

a so-called ponderomotive acceleration that will be proportional to the gradient of the square of the electrical field strength, *viz.*

$$\ddot{\mathbf{R}} = -\left(\frac{e}{2m\omega}\right)^2 \nabla \mathbf{E}^2 = -\nabla\left(\frac{\mathbf{v}_\omega^2}{4}\right) \qquad (10)$$

The vector square notation is here understood as:

$$\mathbf{E}^2 = \mathbf{E}\bullet\mathbf{E}^* \qquad (11)$$

A simplistic explanation of the ponderomotive force is that the oscillating electron moves farther during the half-cycle when it is moving from a region with a strong field to a region with a weak field than vice versa, resulting in a net drift when averaged over a cycle.

The ponderomotive approximation is generally good when the oscillation amplitude is small compared to the structure size and the field inhomogeneity scale length.

The square of the electrical field and the related ponderomotive force lines for the two-wire line are plotted in Fig. 6. The curves are known as Cassini ovals and *stelloïdes*, respectively.

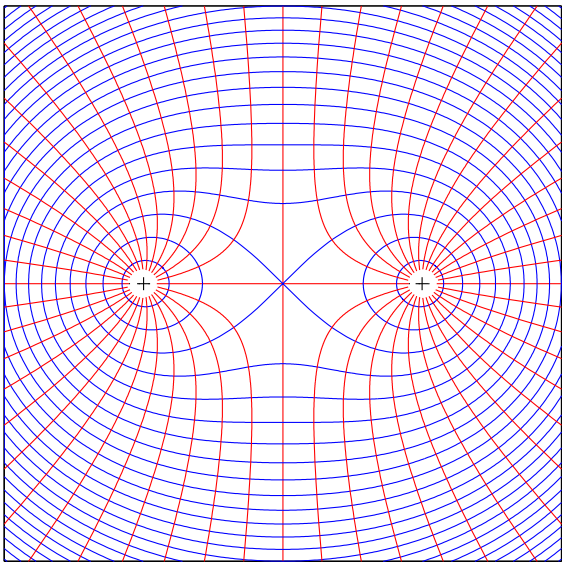

Figure 6. The isophotes for the field strength (blue) and the ponderomotive field lines (red) generated by two filamentary line charges.

Knowing the field and thus the equations of motion enables a semi-analytical approach where a numerical solution of the ponderomotive part is used.

However, there is a higher-level analytical approach that can be used to gain even more insight into the electron ballistics.

By integrating the equations of motion we get an energy conservation relation:

$$\mathbf{v}_d^2 + \tfrac{1}{2}\mathbf{v}_\omega^2 = Const \qquad \mathbf{v}_d = \dot{\mathbf{R}} \qquad (12)$$

The drift velocity can now be found as a function of the initial conditions and the local electrical field strength. The time has disappeared as an explicit parameter, which is very convenient.

3.2. Secondary Emission Yield (SEY) Model

A necessary, but not sufficient, condition for multipactor breakdown is to have a net gain in the number of electrons for a round-trip. Essentially this is the condition that the product of the secondary electron emission yields of the two surfaces should exceed any electron losses due to geometrical factors.

An empirical SEY model similar to one devised by Vaughan [9] has been used in our analysis:

$$\sigma(\varepsilon) = \sigma_m \left[\varepsilon \exp(1-\varepsilon)\right]^{\alpha(\varepsilon)} \qquad (13a)$$

$$\varepsilon = \frac{\frac{1}{2} m v_{imp}^2}{W_m} \qquad \alpha(\varepsilon) = \begin{cases} 0.62 & \varepsilon \le 1 \\ 0.25 & \varepsilon > 1 \end{cases} \qquad (13b)$$

The parameter ε here represents a normalized impact energy, wherein the normalization energy, W_m, corresponds to the maximum secondary emission yield, σ_m.

Representative empirical parameters for silver are W_m=519 eV and σ_m=2.22, and the resulting SEY curve is shown in Fig. 7. A range of impact energies will generate an SEY larger than unity.

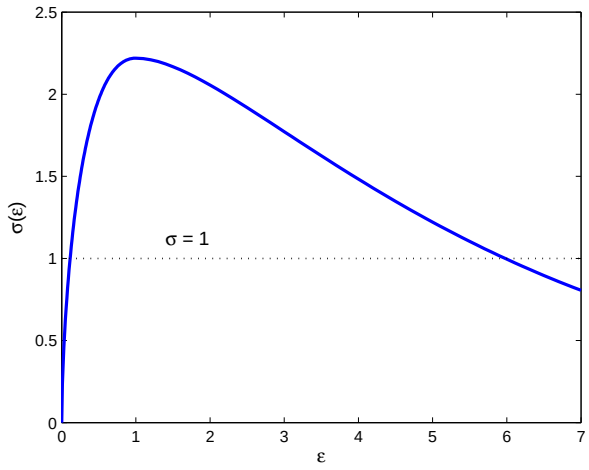

Figure 7. The SEY model for silver.

3.3. Geometrical Dilution Model

At the emission of a secondary electron from the surface, the initial conditions are mainly set by the surface electric field. In our two-wire case we assume perfect electric conductors (PEC), and then it is known that the tangential E-field is zero on the conductor. Hence, the E-field, and thus the initial acceleration, will be normal to the conductor surface. With the circular cross-section, all initial velocity lines converge on the center of the conductor, see Fig. 8.

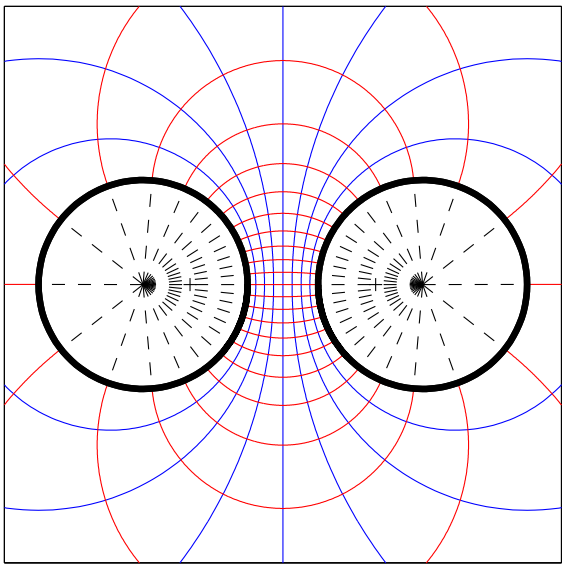

Figure 8. The electrical field lines (red circles) on the conductor surfaces appear to emanate from the center (surface normals).

We now consider a bunch of electrons emitted from an infinitesimal surface element dA_{emi}. When impacting the other surface the electron bunch will cover a surface element dA_{imp} (see Fig. 9). Our simplistic model of straight trajectories normal to the surface thus trivially gives the ratio between the electron densities, n_A, at the two surfaces as:

$$\frac{n_{A,imp}}{n_{A,emi}} = \frac{dA_{emi}}{dA_{imp}} = \frac{R_{emi}}{R_{emi} + d} \tag{14}$$

For a round-trip along the symmetry line in our two-wire geometry we would thus have an equivalent total dilution of

$$\frac{1}{\left(1 + d/R_1\right)\left(1 + d/R_2\right)} \tag{15}$$

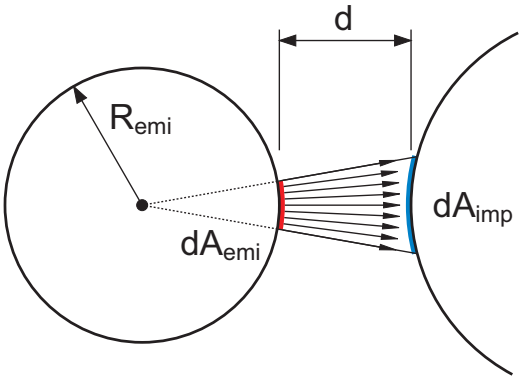

Figure 9. The geometrical dilution effect on a bunch of emitted electrons.

For the coaxial case, the equivalent dilution factor collapses to unity due to focusing from the outer conductor (the radius is negative).

The question is now how realistic this simplistic model is. By plotting the ponderomotive force field lines as in Fig. 10, we can see that these field lines appear to emanate from a point that is located closer to the surface. The ponderomotive forces would increase the deflection of the electrons away from the nominal trajectory, and the straight line approach is hence a conservative bound for the geometrical electron dilution.

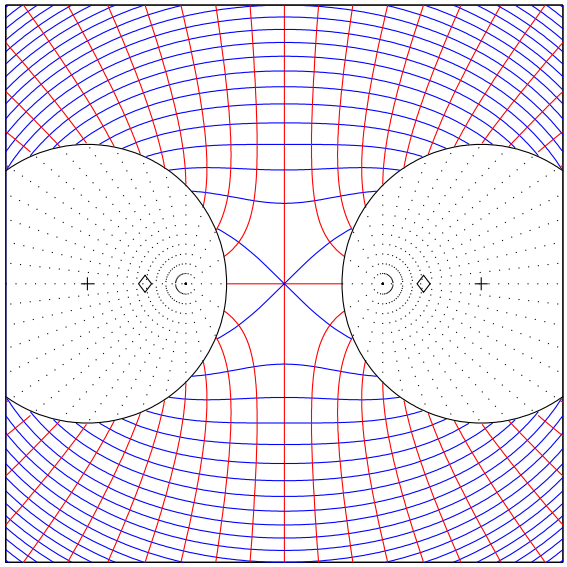

*Figure 10. The ponderomotive field lines (*stelloïdes*) on the conductor surfaces appear to emanate from a point that is located closer to the surface.*

The geometrical dilution is essentially a measure of the walk-off that is produced by the field inhomogeneity across the structure.

A conservative condition for multipactor would thus be:

$$\frac{\sigma_1\left(v_{1,imp}\right)\sigma_2\left(v_{2,imp}\right)}{\left(1+d/R_1\right)\left(1+d/R_2\right)} > 1 \tag{16}$$

Since the maximum SEY is limited, we can assign an upper limit to the relation:

$$\frac{\sigma_{m1}\sigma_{m2}}{\left(1+d/R_1\right)\left(1+d/R_2\right)} > 1 \tag{17}$$

Assuming the same SEY properties for both surfaces, we can now plot the limiting lines in the parameter plot as in Fig. 11:

$$\left(1+d/R_1\right)\left(1+d/R_2\right) = \sigma_m^2 \tag{18}$$

Above these lines the geometrical dilution will prohibit multipactor.

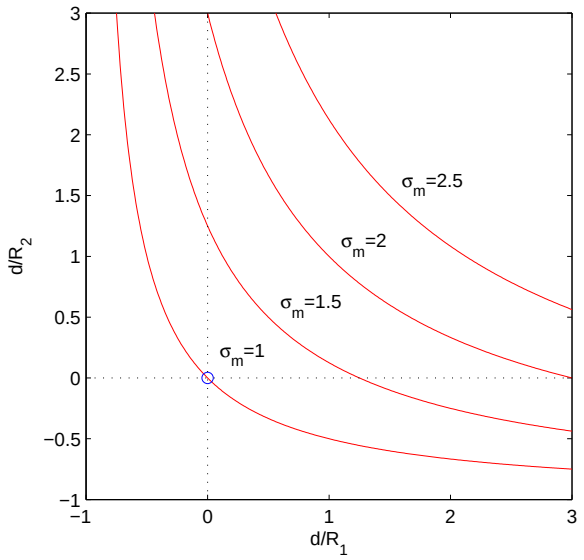

Figure 11. The SEY limit curves for geometrical dilution.

One should note that the geometrical dilution factor can be extended to a three-dimensional case as well. A doubly curved surface with the principal radii of curvature denoted by ρ_ξ and ρ_η will yield a one-way dilution factor of

$$\frac{1}{\left(1+d/\rho_\xi\right)\left(1+d/\rho_\eta\right)} \tag{19}$$

3.4. Double-Sided Multipactor Conditions

We assume that the emission velocity is negligible, *i.e.* the sum of the instantaneous oscillation velocity and the initial drift velocity is approximately zero:

$$-v_{\omega,emi}\sin\varphi_o + v_{d,emi} \approx 0 \tag{20}$$

The initial drift velocity is then limited by:

$$v_{d,emi}^2 \le v_{\omega,emi}^2 \tag{21}$$

The energy conservation relation in Eq. 12 yields:

$$v_{d,imp}^2 + \tfrac{1}{2}v_{\omega,imp}^2 = v_{d,emi}^2 + \tfrac{1}{2}v_{\omega,emi}^2 \tag{22}$$

Combining these relations gives the following bound:

$$\begin{aligned} v_{d,imp}^2 &= v_{d,emi}^2 + \tfrac{1}{2}\left(v_{\omega,emi}^2 - v_{\omega,imp}^2\right) \\ &\le \tfrac{1}{2}v_{\omega,emi}^2\left[3-\left(v_{\omega,imp}/v_{\omega,emi}\right)^2\right] \end{aligned} \tag{23}$$

From this follows that the drift velocity will be zero if

$$\frac{v_{\omega,imp}}{v_{\omega,emi}} = \frac{E_{imp}}{E_{emi}} = \sqrt{3} \tag{24}$$

Thus, if the ratio of the field strengths on the conductor surfaces exceeds this limit, the electron will not impact with the second surface. The conditions for double-sided multipactor along the symmetry line for the two-wire line are then given by:

$$\frac{1}{\sqrt{3}} < \frac{2+d/R_2}{2+d/R_1} < \sqrt{3} \tag{25}$$

These conditions are conveniently plotted as straight lines in the parameter plot, see Fig. 12.

Combining the above graph with the previous graph of geometrical dilution, we get Fig. 13. The curves enclose an area outside which double-side multipactor is impossible for the parameter ranges considered in this paper.

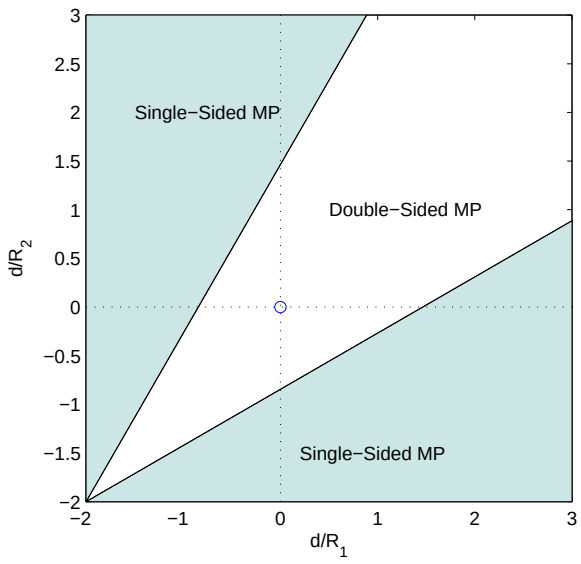

Figure 12. The allowable region for double-sided multipactor.

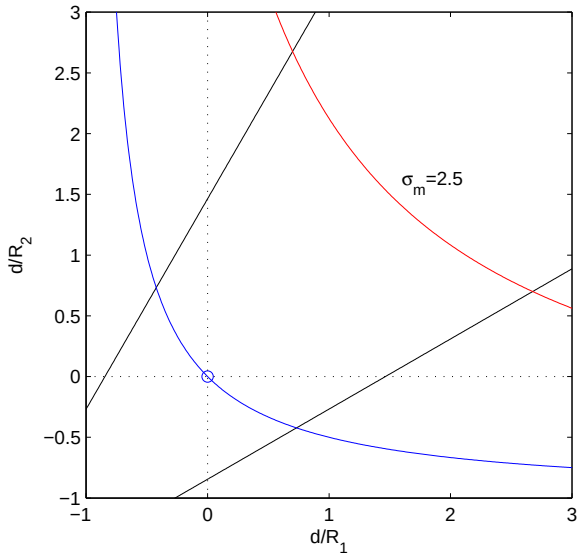

Figure 13. The combined graph for the various regions.

3.5. Multipactor Threshold Calculations

The previous sections have dealt with the different limit cases, but it is also possible to analytically compare the multipactor threshold to that of the parallel plate case. The methodology of this solution is detailed in [10], and only the main points will be repeated here for convenience.

The round-trip condition will be given by the products of the geometrical dilutions and SEYs in each direction:

$$\frac{\sigma\left(\varepsilon_1\left(\psi\right)\right)}{\left(\frac{d}{R_1}+1\right)}\frac{\sigma\left(\varepsilon_2\left(\psi\right)\right)}{\left(\frac{d}{R_2}+1\right)}=1 \tag{26}$$

The normalized impact energies ε_1 and ε_2 are here geometry dependent functions of a parameter ψ, which is the ratio of the multipactor threshold voltage compared to the one for the parallel plate case. Numerical root search is used to find the ψ that solves Eq. 26 together with the SEY model $\sigma(\varepsilon)$ as defined in Eq. 13.

We now need to find the geometry dependent impact energy functions. A conservative bound for the impact velocity could be the sum of the drift velocity and the peak oscillation velocity. However, a more suitable approach would be to average the impact velocity for all possible phase angles. The averaged impact velocity as a function of the drift and peak oscillation velocities can in that case be shown to be:

$$\left\langle v_{imp}\right\rangle=\frac{\int v^2dt}{\int v\,dt}=v_{\omega,imp}\cdot\Theta\left(\frac{v_{d,imp}}{v_{\omega,imp}}\right) \tag{27a}$$

$$\Theta\left(\kappa\right)=\frac{\left(\kappa^2+\frac{1}{2}\right)\varphi_\kappa+2\kappa\sin\varphi_\kappa+\frac{1}{4}\sin 2\varphi_\kappa}{\kappa\varphi_\kappa+\sin\varphi_\kappa} \tag{27b}$$

$$\varphi_\kappa=\begin{cases}\arccos\left(-\kappa\right) & \kappa<1\\ \pi & \kappa\geq 1\end{cases} \tag{27c}$$

Using this estimate for the impact velocity, the normalized energies for the two-wire case can be written as:

$$\varepsilon_1=\Omega\left(\psi,\frac{d}{R_1},\frac{d}{R_2}\right)\qquad\varepsilon_2=\Omega\left(\psi,\frac{d}{R_2},\frac{d}{R_1}\right) \tag{28a}$$

$$\Omega(\psi,a,b)=\left[\Theta\left(\sqrt{\frac{3}{2}\left[\frac{b+2}{a+2}\right]^2-\frac{1}{2}}\right)\Big/\Theta\left(1\right)\right]^2 \cdot\varepsilon_{pp}\psi^2\,\frac{b+2}{a+2}\,\Xi\Big(\left(a+2\right)\left(b+2\right)-4\Big) \tag{28b}$$

$$\Xi\left(x\right)=x\Big/\left[\operatorname{arccosh}\left(1+x/2\right)\right]^2 \tag{28c}$$

The parameter ε_{pp} in Eq. 28b is the normalized impact energy for the parallel plate threshold case. It is not geometry dependent, and is found by numerical root search of the following equation:

$$\sigma\left(\varepsilon_{pp}\right)=1\qquad\varepsilon_{pp}<1 \tag{29}$$

The numerical results for the two-wire TEM line multipactor threshold as a function of the geometrical parameters are shown in Fig. 14. The SEY limit curve (as in Fig. 11) is also plotted in the figure. It is seen that the solution does not "fill" the region entirely. This is due to the fact that both SEY functions cannot be at the maximum value simultaneously for an asymmetric case.

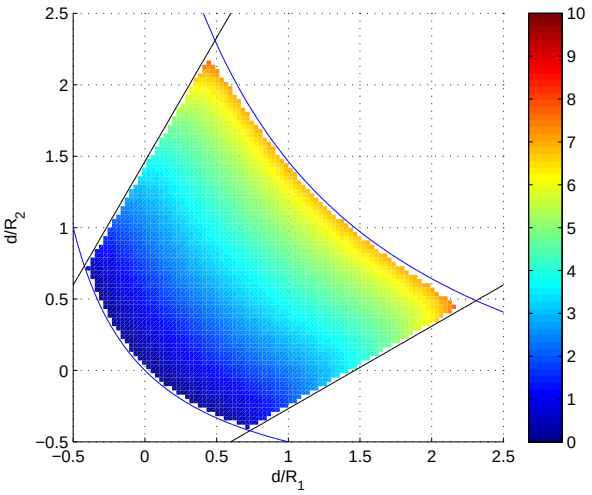

Figure 14. The relative two-wire TEM line multipactor susceptibility (compared to the parallel plate case) for the presented model with σ_m=2.22. Pseudo-color plot with a logarithmic scale: $20 \cdot \log_{10} \left| V_{th} / V_{pp} \right|$

4. CONCLUSIONS

An analysis methodology has been developed to assess the multipactor susceptibility of two-wire TEM transmission lines. The model provides an excellent insight into the geometry dependent multipactor mechanisms, and the formalism is likely to be possible to be extended to other structures.

The presented model introduces several new effects that are present in curved geometries. Using the ponderomotive force concept, one can rule out double-sided multipactor for two-wire systems with large differences in radii, simply because electrons ejected from one side will not reach the other. For convex geometries, a bunch of electrons will undergo spreading between successive rounds of impact, emission, and transport between the surfaces. For a given secondary emission yield, this dilution effect makes double-sided multipactor impossible for conductor radii less than a limit value.

Future work will be concentrated on numerical corroboration of the presented theory, as well as experimental verification by tests on reference structures of the two-wire line type.

5. ACKNOWLEDGMENTS

This work has been supported by the Russian Foundation for Basic Research through Grant No. 09-02-97024-a and by the Swedish National Space Technology Research Program (NRFP).

6. REFERENCES

1. A.M. Pérez, C. Tienda, C. Vicente, S. Anza, J. Gil, B. Gimeno, V. E. Boria, and D. Raboso, "Prediction of Multipactor Breakdown Thresholds in Coaxial Transmission Lines for Traveling, Standing, and Mixed Waves", *IEEE Trans. Plasma Sci.*, Vol. 37, No. 10, pp. 2031-2040, Oct. 2009

2. R. Udiljak, D. Anderson, M. Lisak, V. E. Semenov, and J. Puech, "Multipactor in a coaxial transmission line, part 1: analytical analysis", *Phys. Plasmas* 14, 033508 (2007)

3. A. G. Sazontov, V. A. Sazontov, and N. K. Vdovicheva, "Multipactor breakdown prediction in a rectangular waveguide: statistical theory and simulation results", *Contrib. Plasma Phys.* 48, 331 (2008)

4. V. E. Semenov, E. I. Rakova, D. Anderson, M. Lisak, and J. Puech, "Multipactor in rectangular waveguides", *Phys. Plasmas* 14, 033501 (2007)

5. A.M. Péres, V.E. Boria, B. Gimeno, S. Anza, C. Vicente, and J. Gil, "Multipactor Analysis in Circular Waveguides", *J. Electromagn. Waves and Appl.*, Vol. 23, No. 11-12, pp. 1575-1583, 2009

6. V. E. Semenov, E. Rakova, R. Udiljak, D. Anderson, M. Lisak, and J. Puech, "Conformal mapping analysis of multipactor breakdown in waveguide irises", *Phys. Plasmas* 15, 033501 (2008)

7. *ECSS-E-20-01A; Space Engineering; Multipaction design and test*, ECSS Secretariat, ESA-ESTEC, 2003

8. B.D. Popović, *Introductory Engineering Electromagnetics*, Addison-Wesley, Reading, Massachusetts, USA (1971)

9. J.R.M. Vaughan, "A new formula for secondary emission yield", *IEEE Trans. Electron Devices*, Vol. 36, No. 9, pp. 1963-1967, Sep. 1989

10. J. Rasch, D. Anderson, J. Johansson, M. Lisak, J. Puech, E. Rakova, and V.E. Semenov, "Microwave Multipactor Breakdown Between Two Cylinders", *IEEE Trans. Plasma Sci.*, Vol. 38, No. 8, pp. 1997-2005, Aug. 2010